

Columns in Reinforced Concrete Buildings Impacted by Tsunami Water-Borne Massive Objects

M.A.K.M. Madurapperuma & A.C. Wijeyewickrema

Tokyo Institute of Technology, Tokyo, Japan



SUMMARY:

The tsunamis generated by the Chile earthquake in February 2010 and Tohoku Pacific Ocean earthquake in March 2011 caused numerous shipping containers in ports to be dislodged and impact on port structures. Hence, characterization of forces on structures due to such impact loads is vital for the design of buildings used for evacuation purposes and other important structures located in tsunami inundation zones. In this paper, reinforced concrete (RC) columns impacted by shipping containers dispersed by a tsunami is considered. The container-column impact analysis is carried out using two types of standard shipping containers and RC columns with square and circular sections. The findings of this study provide useful insight into container-column impact behavior and will be useful when revising existing design guidelines on tsunami loads.

Keywords: Numerical simulation; Reinforced concrete columns; Tsunamis; Water-borne shipping containers

1. INTRODUCTION

One of the major threats to structures in the tsunami inundation zone is impact of massive objects carried by the tsunami flow. The tsunamis generated by the Chile earthquake ($M_w = 8.8$) in February 2010 and Tohoku Pacific Ocean earthquake ($M_w = 9.0$) in March 2011 caused numerous shipping containers in ports to be dislodged and impact on port structures (Chock et al. 2011; Robertson et al. 2010). Hence, characterization of forces on structures due to impact of tsunami water-borne shipping containers is vital for the design of buildings used for evacuation purposes and other important structures located in tsunami inundation zones. The design guidelines ASCE 7-10 (ASCE 2010) and FEMA P646 (FEMA 2008) provide formulae to estimate the impact force on structures due to impact of tsunami water-borne massive objects. However, these formulae are based on simplified linear elastic analyses, and the estimated impact forces for shipping containers from each formula differ by an order of magnitude; indicating that the parameters given in the guidelines for the estimation of impact force for tsunami water-borne shipping containers should be reconsidered.

There have been very few previous studies on container impact on structures. Madurapperuma and Wijeyewickrema (2012a) considered impact of a 20' container on an RC building modeled with nonlinear beam-column elements with fiber-based section discretization, using impact force-time histories obtained from a high-fidelity finite element analysis. Madurapperuma and Wijeyewickrema (2012b) proposed formulae for the estimation of peak impact force on square and circular RC columns impacted by a 20' container. Here, high-fidelity finite element models were considered for container-column impact analysis, and results for sideways impact of the container were used to obtain the proposed formulae.

In the present study, impact response of RC columns is considered using 20' and 40' general purpose standard shipping containers which are widely used for maritime freight transport. The container models include all significant parts with associated structural details, and RC columns with square and circular sections are considered. Different impact configurations are considered in the analysis. Damage to the impacted column is assessed using a damage index characterized by degradation of axial load carrying capacity.

2. FINITE ELEMENT MODELING OF SHIPPING CONTAINER-RC COLUMN IMPACT

The explicit Lagrangian finite element code LS-DYNA (2007), used extensively for impact problems, is used.

2.1. Shipping Container Models

The 20' and 40' general purpose standard shipping containers that are widely used for maritime freight transport are considered to investigate impact response and damage assessment of RC columns. As shown in Fig. 2.1, the 20' container model has 2 mm thick corrugated panels which are connected to top side rails with hollow square sections ($58 \times 58 \times 3$ mm). The floor of the container consists of two main bottom side rails with channel sections ($155 \times 54 \times 4.5$ mm) and 19 cross members with channel sections ($118 \times 43 \times 4$ mm). The container has four corner posts with hollow rectangular sections ($105 \times 58 \times 6$ mm). The surface of the wall panel is set back by 10 mm and is not flush with the outer edges of the side rails and corner posts. This description follows specifications for a 20' steel container given by Containex (2004). The 40' shipping container has a similar structural framework as the 20' container but with additional cross members and larger section sizes for corner posts ($178 \times 156 \times 6.5$ mm). As shown in Fig. 2.2, the floor of 40' container consists of additional stiff beams with hollow sections (two longitudinal beams with dimensions of $155 \times 121 \times 5$ mm and a transverse beam with dimensions of $155 \times 150 \times 5$ mm) and cross members of channel sections ($102 \times 20 \times 4$ mm) close to the front end of the container (Magellan 2010).

The 4-node Belytschko-Tsay shell elements with one-point quadrature are used to model all parts of the containers, since this element is very robust under severe distortion (Belytschko et al. 2000). The 20' container model consists of 22,025 nodes and 22,681 elements, and the 40' container model has 38,176 nodes and 38,591 elements. The material model MAT_PLASTIC_KINEMATIC (MAT_003) is used to represent material behavior of the containers. The material properties used in the analysis are density 7850 kg/m^3 , Young's modulus 210 GPa, Poisson's ratio 0.3, yield strength 355 MPa, tangential hardening modulus 1000 MPa, and failure strain 22%, based on material tests given in container specifications (Containex 2004). Strain rate effects are considered using the Cowper and Symonds constitutive relation with coefficients $D = 40.4 \text{ s}^{-1}$ and $q = 5$ (Jones 1989).

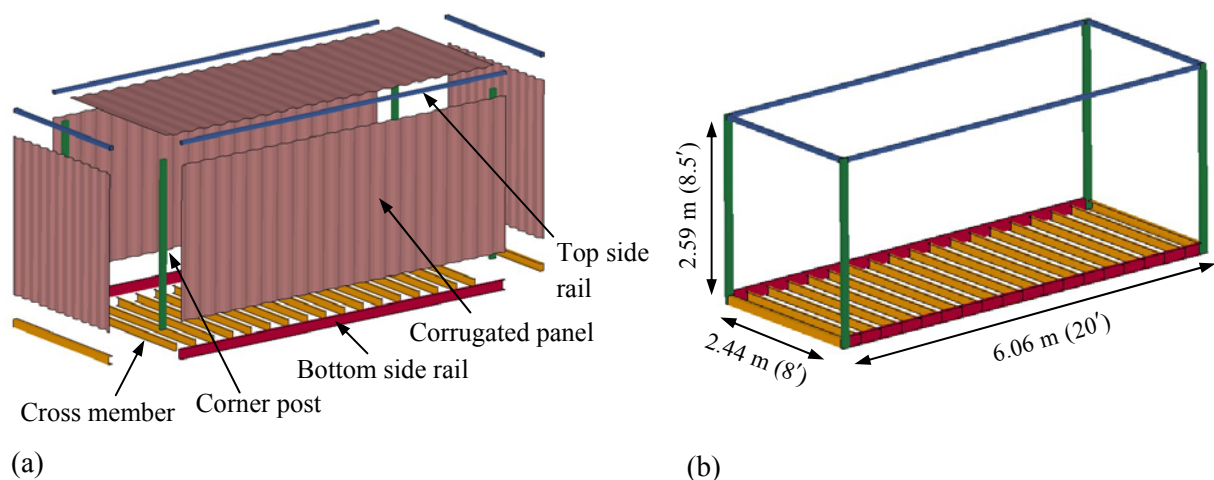


Figure 2.1. The 20' shipping container model: (a) structural members, (b) structural framework.

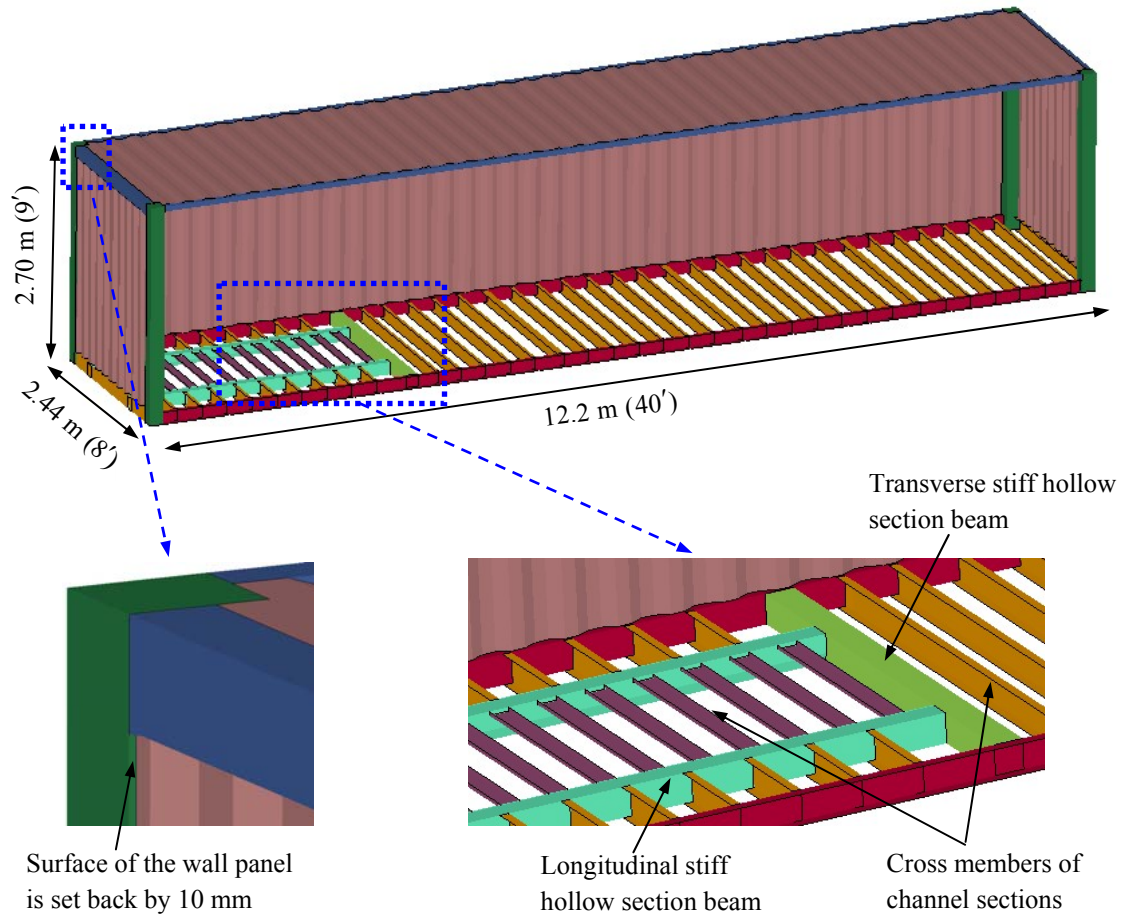


Figure 2.2. The 40' shipping container model with the side corrugated panel removed for visualization of the floor structure.

2.2. RC Column Models

A square column ($300 \text{ mm} \times 300 \text{ mm}$) and a circular column $\phi = 340 \text{ mm}$ are chosen to have nearly the same cross-sectional area $A_g = 0.09 \text{ m}^2$. The columns have height $H = 4 \text{ m}$, compressive strength of concrete $f'_c = 40 \text{ MPa}$, and mass density of concrete $\rho_c = 2400 \text{ kg/m}^3$. Details of longitudinal and transverse reinforcement are shown in Fig. 2.3(a). The structural details of the columns correspond to a 3-story building used for public assembly, and more details on the design considerations of these columns are given in Madurapperuma and Wijeyewickrema (2012b).

The constant stress 8-node solid elements with one-point quadrature and the Hughes-Liu beam elements are used to represent concrete and reinforcing steel, respectively (Fig. 2.3a). Each concrete element in the square column is a 25 mm cube, and an element length of 25 mm in axial direction is used in the circular column. The longitudinal and transverse reinforcement are modeled using 25 mm long beam elements. The square column model consists of 32,745 nodes and 26,496 solid elements, and the circular column model has 36,260 nodes, 31,464 solid elements, and both the columns have 2,432 beam elements. The constraints provided by the foundation and the upper end at the beam-column joint are included in the model as shown in Fig. 2.3(b). The nodes on outer vertical surfaces of the foundation and upper end are constrained horizontally and nodes on bottom surface of the foundation are constrained vertically. The material model MAT_CONCRETE_DAMAGE_REL3 (MAT_072R3) is selected as the constitutive model for concrete where compressive strength of concrete f'_c is used to generate the remaining material

parameters. This KCC material model (Crawford and Malvar 2006) has been extensively used for the investigation of RC structural response to blast and impact loads and has performed well in simulating experimentally observed behavior (Malvar et al. 1997; Tu and Lu 2009). The effect of strain rate on concrete material is considered using the formula given by CEB-FIP code (CEB 1993) for compressive strength and the formula given by Malvar and Ross (1998) for tensile strength. The material model MAT_PIECEWISE_LINEAR_PLASTICITY (MAT_024) is used to model longitudinal and transverse reinforcement. The material properties of the longitudinal reinforcement are density 7850 kg/m³, Young's modulus 200 GPa, Poisson's ratio 0.3, yield stress 475 MPa, tangent modulus 2.0 GPa, and failure strain 12%. For the transverse reinforcement yield stress 330 MPa, tangent modulus 1.5 GPa, and failure strain 15% are used, with other properties similar to the longitudinal reinforcement. Since the yield stress of reinforcing bar increases at high strain rates, strain rate effects on reinforcement are considered using the formula proposed by Malvar (1998). The bond behavior between concrete and reinforcing bars is taken into account by using the one-dimensional slide line contact model, CONTACT_1D. In the slide line contact model the interfacial shear force increases linearly up to a maximum and then decay exponentially with the increase of slip between concrete and reinforcement. In addition to the compressive strength of concrete and the bar diameter, three parameters used to define the interfacial shear force-slip relation bond shear modulus $G_s = 34 \text{ MPa/mm}$, maximum elastic slip $s_{\max} = 0.69 \text{ mm}$, and exponential coefficient $h_{\text{dmg}} = 0.18$ are taken from Shi et al. (2009). Material erosion through removal of highly distorted concrete elements from the column model is incorporated using the MAT_ADD_EROSION option. Two erosion criteria, viz., principal strain and shear strain are considered to simulate material failure caused by crushing and spalling of concrete during container impact. It is found from a separate analysis of container-column impact that the appropriate values for the principal strain and shear strain are 0.15 and 0.9, respectively.

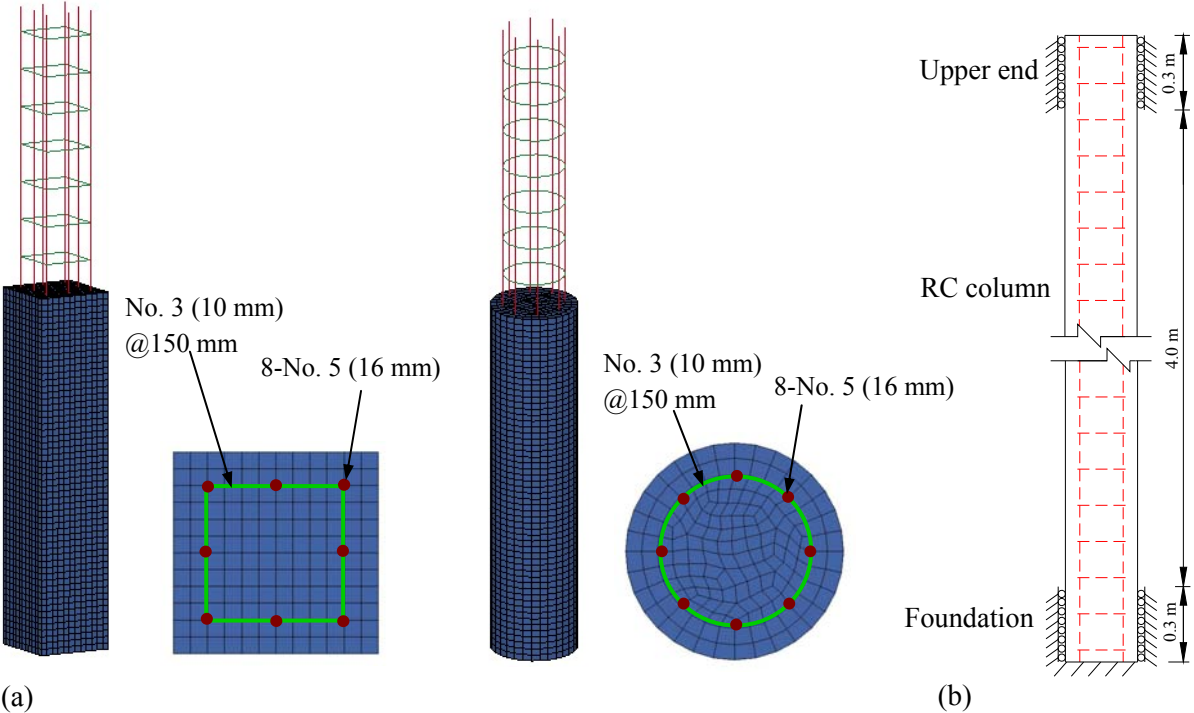


Figure 2.3. (a) RC column finite element models and (b) constraints provided at the foundation and the upper end of columns.

2.3. Contact Modelling and Hourglass Control

Contact between the container and concrete in the column, and *self-contacts* among the container components such as corrugated panels and cross members are defined using the contact type

CONTACT_AUTOMATIC_SINGLE_SURFACE. The coefficient of friction between contact surfaces is taken as 0.3. To overcome spurious singular modes, i.e., hourglass modes, in shell and solid elements, a fine mesh together with hourglass control procedures available in LS-DYNA are used. Here the maximum hourglass energy is not more than 5% of total energy in all simulations. Since the hourglass energy is low this ensures accuracy of the numerical results (Belytschko et al. 2000).

3. SHIPPING CONTAINER-RC COLUMN IMPACT ANALYSIS AND RESULTS

3.1. Analysis Procedure

Prior to container impact, an axial load of $P_N = 1000 \text{ kN}$ ($0.28 f'_c A_g$) corresponding to the load obtained from a 3-story building used for public assembly, is applied to simulate gravity loads acting on the column. Then the container impacts the column and data related to the damage state of the column is obtained. The residual axial load carrying capacity is estimated by increasing the axial load on the damaged column until axial failure of the column. Six different container-column impact configurations are considered. Figure 3.1 shows 40' container impacting square column, and the same six configurations are used for the container impacting circular column. These container-column impact configurations lead to different impact conditions where in some cases relatively stiff members of the container directly resist container deformation. Although the stiff hollow beams (shown in configurations L2 and T2) are not provided in the 20' container, similar impact configurations are considered for comparison purposes. Both the containers approach at a height of 0.05 m above the ground level and impact with the square and circular columns.

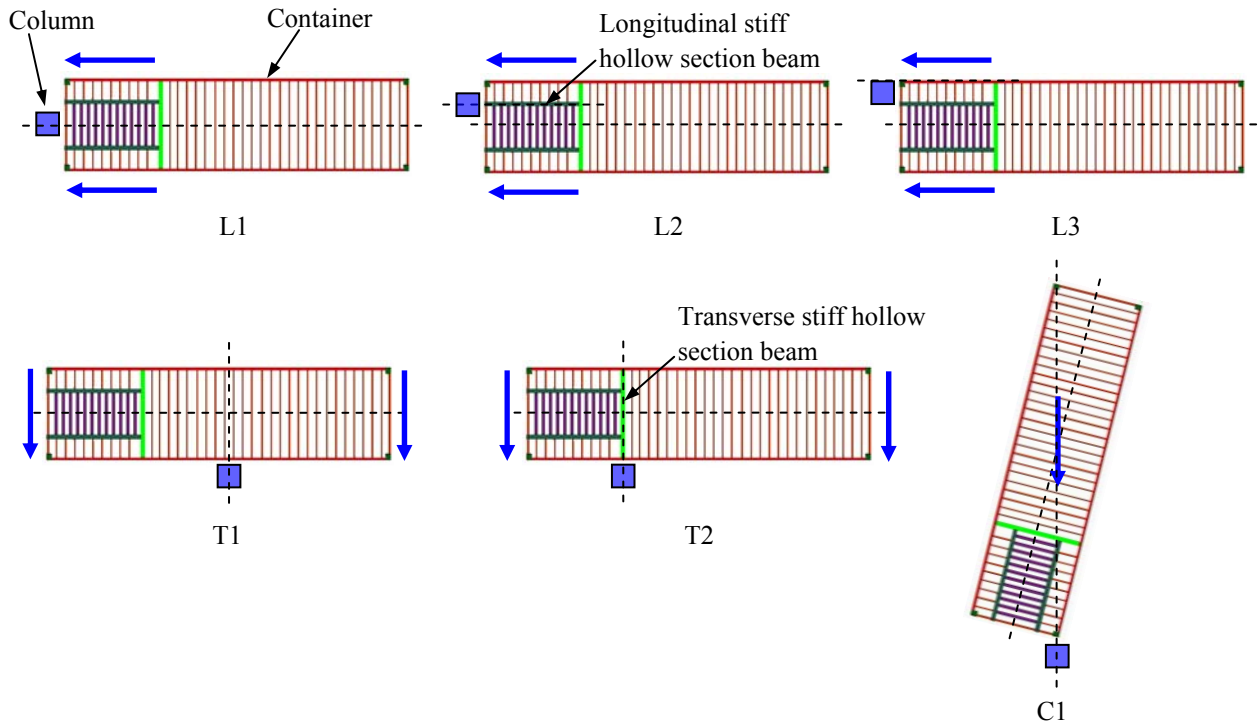


Figure 3.1. The 40' container-column impact configurations where the direction of container movement is indicated by the arrows: L1- center of transverse side rail in line with center of column; L2- center of longitudinal stiff hollow section beam in line with center of column; L3- outer surface of container corner post and column face is flush; T1- center of longitudinal side rail in line with center of column; T2- center of transverse stiff hollow section beam in line with center of column, and C1- corner post in line with center of column.

3.2. Impact Force on RC Columns

Peak impact force for both types of columns are compared with the estimated impact forces using ASCE 7-10 in Figs. 3.2 and 3.3. As noted earlier, the peak impact forces estimated using FEMA P646 are too conservative and differ by an order of magnitude and are not shown in these figures. Peak impact forces for both columns increase with the increase of container velocity. Peak impact forces are shown for the container velocities where the column is able to sustain the axial load and has not collapsed. In general, for all impact configurations, peak impact force of square column is larger than that of circular column because the square column is in contact with a wider area of the impacting container leading to higher impact forces. For the 20' container as shown in Fig. 3.2, the column is able to sustain the axial load without collapse only for the impact configurations L1 and L2. For a given velocity the peak impact force for the 40' container is higher than that for the 20' container and other than the configuration L1, both the columns are not able to sustain the axial load and have collapsed for higher container velocities (Fig. 3.3). This is expected as 40' container is 1.7 times heavier than 20' container and there are stiff beams in the floor system of 40' container in addition to regular cross members. In particular, the 40' container in configurations L2, L3, and C1 where stiff beams in the container floor directly resist container deformation, apply higher forces on both columns compared to other configurations. It is remarkable that peak impact forces for 40' container in configuration L2 impacting both columns, are more than three times the corresponding values for 20' container although the mass of the 40' container is about 1.7 times larger than the 20' container. This implies that not only the mass of the container but also differences in the structural system of these containers are significant.

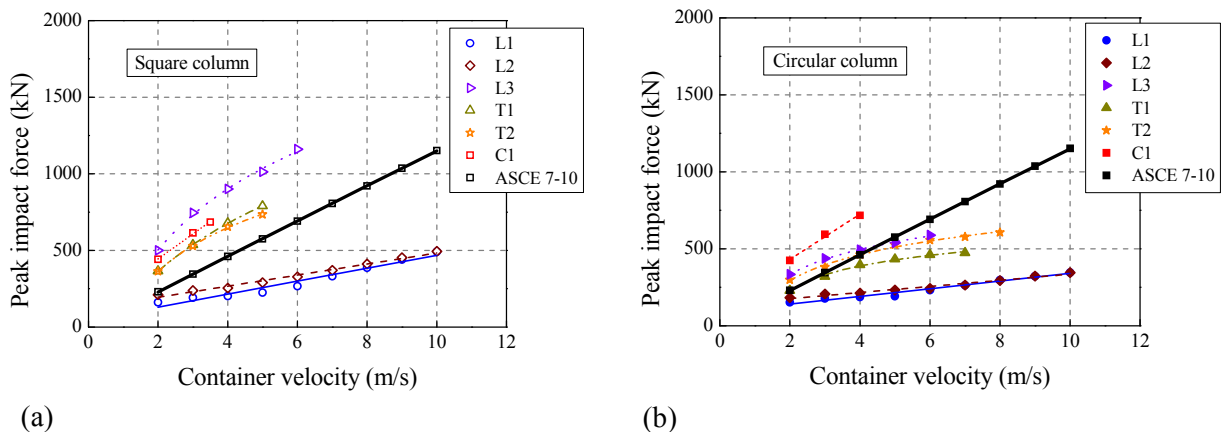


Figure 3.2. Peak impact force for different impact configurations of 20' container: (a) square column and (b) circular column. The impact force estimated using ASCE 7-10 is also shown.

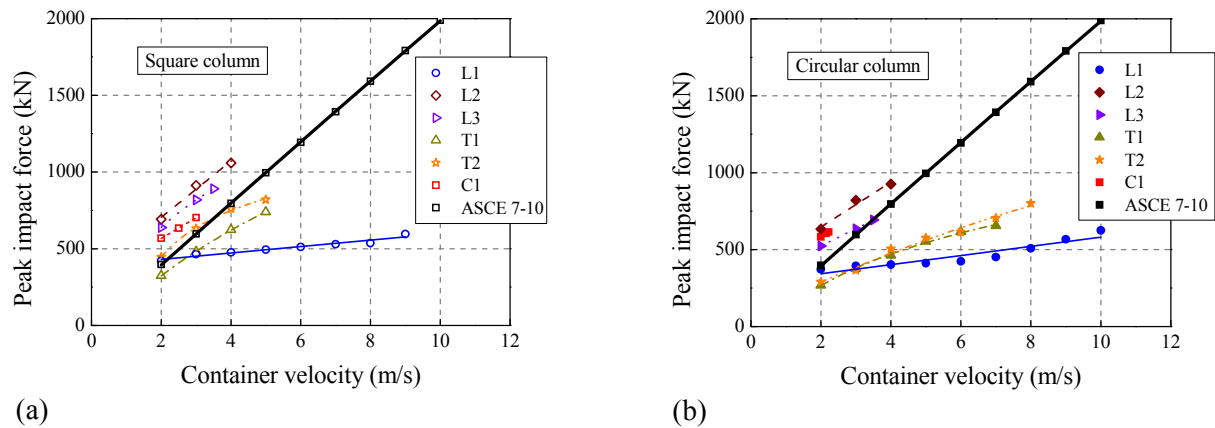


Figure 3.3. Peak impact force for different impact configurations of 40' container: (a) square column and (b) circular column. The impact force estimated using ASCE 7-10 is also shown.

3.3. Damage to RC Columns

Figures 3.4 and 3.5 show evolution of damage to columns during container impact for square and circular columns, respectively. Here, the 40' container in configuration C1 is considered to impact at 4 m/s which leads to collapse of these columns. Due to the impact, part of the initial kinetic energy of the container is transferred to the column. The amount of energy transfer depends on stiffness and inertia of both the container and column. Local deformation in the column occurs due to crushing and spalling of concrete in the vicinity of contact regions, and the erosion model incorporated in the present analysis is able to identify these locations. This is followed by the shear failure of the column with a failure surface across the thickness of the column. The shear force close to the foundation of the square column is 530 kN before shear failure, which is about 2.5 times the static shear capacity 209 kN of the square column. In the case of the circular column, the shear force close to the foundation is 502 kN before shear failure, which is about 1.9 times the static shear capacity 266 kN of the circular column. Here the static shear capacities are obtained without strength reduction factor and including the effect of column axial load using the ACI code (ACI 2008). The increase in the shear force capacity could be caused by strength enhancement in concrete and reinforcement due to strain rate effects and inertia of the column. As shown in the figures, onset of shear failure close to the foundation causes abrupt axial failure of both the columns.

The damage index D used to evaluate degree of damage of the impacted columns is defined by,

$$D = \frac{(P_N^{undamaged} - P_N^{damaged})}{(P_N^{undamaged} - P_N)}, \quad (3.1)$$

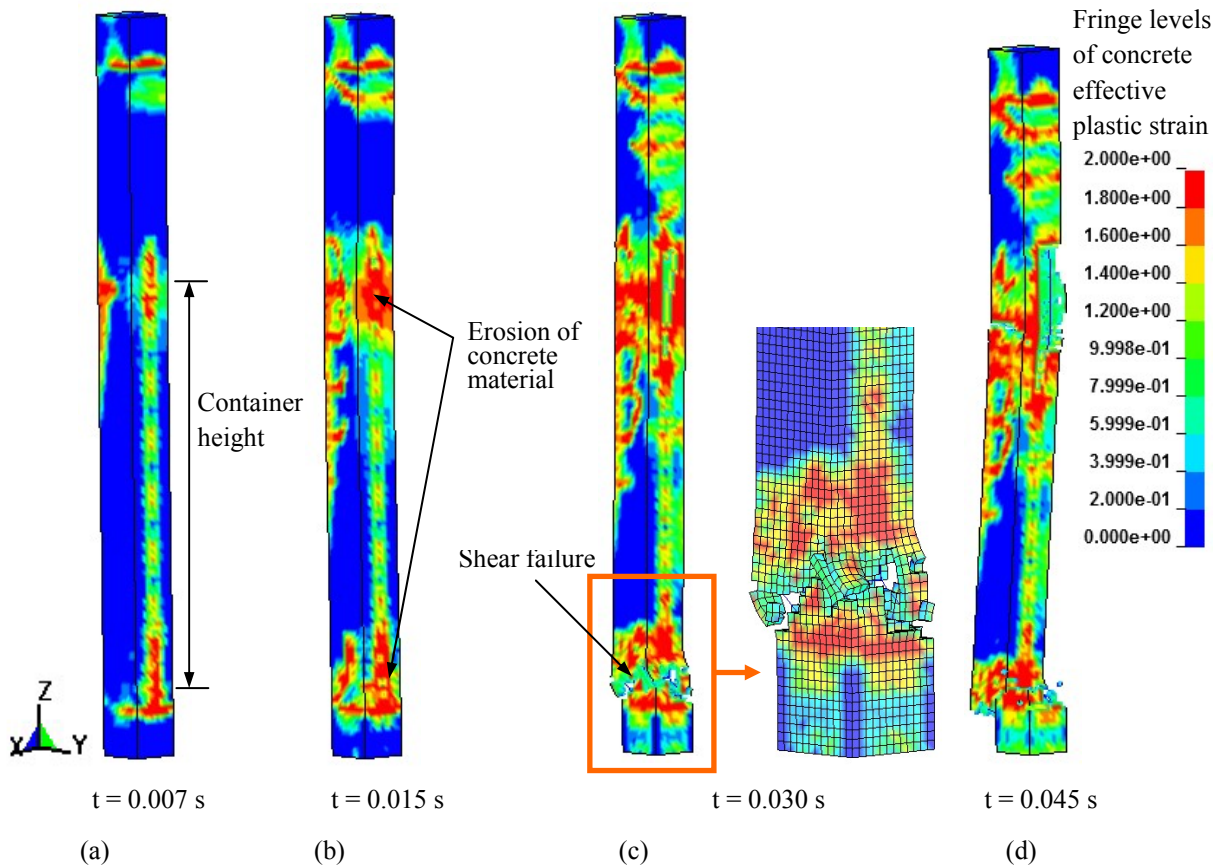


Figure 3.4. Damage patterns of square column for impact of 40' container at 4 m/s along the Y-axis for configuration C1: (a) at peak force, (b) erosion of concrete material from impact face, (c) shear failure at the foundation and close-up view in the vicinity of shear failure, and (d) axial failure.

where P_N is axial load on the column due to gravity loads, $P_N^{damaged}$ and $P_N^{undamaged}$ are axial load carrying capacities of damaged and undamaged columns, respectively. The $P_N^{damaged}$ is obtained using the analysis procedure discussed in Section 3.1 and $P_N^{undamaged}$ is obtained using a separate analysis where the column is subjected to axial compression until failure. The damage index varies from 0 where the column is undamaged, to 1 where the column has lost its ability to sustain applied axial load. Figures 3.6 and 3.7 show variation of damage index for the columns impacted by 20' and 40' containers, respectively. For impact by the 20' container at higher velocities, the column could not sustain the axial load and have collapsed for configurations L3, T1, T2, and C1 (Fig. 3.6). In general, strength degradation and subsequent axial failure is faster in the square column compared to the circular column. This is expected as the peak impact force on the circular column is lesser than that of square column for the same container velocity, and more importantly, the circular column provides better core concrete confinement. It is found for both containers that damage to columns is severe when containers impact in configuration C1 where the edge of the corner post first come into contact with the columns. The impact configurations L3 and L2 also cause significant damage to columns impacted by 40' container due to the stiff beams in the floor system. In general, damage to columns caused by impact of both the containers in configurations T1 and T2 is nearly the same. On the other hand, both containers experience severe damage for configuration L1 as there is no stiff member to resist the container deformation. Here, the most of initial kinetic energy is absorbed by the container for inelastic deformation, and energy transfer to the column is reduced causing less damage to the column.

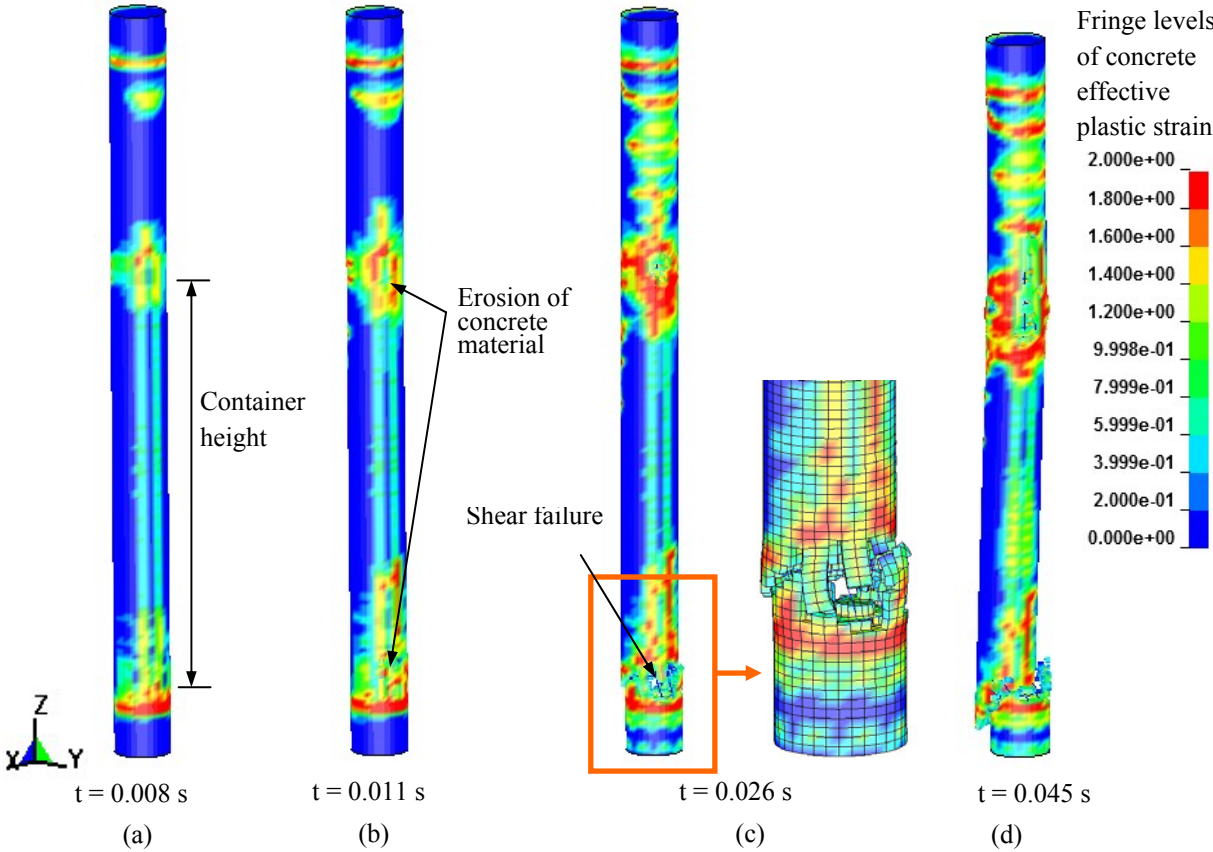


Figure 3.5. Damage patterns of circular column for impact of 40' container at 4 m/s along the Y-axis for configuration C1: (a) at peak force, (b) erosion of concrete material from impact face, (c) shear failure at the foundation and close-up view in the vicinity of shear failure, and (d) axial failure.

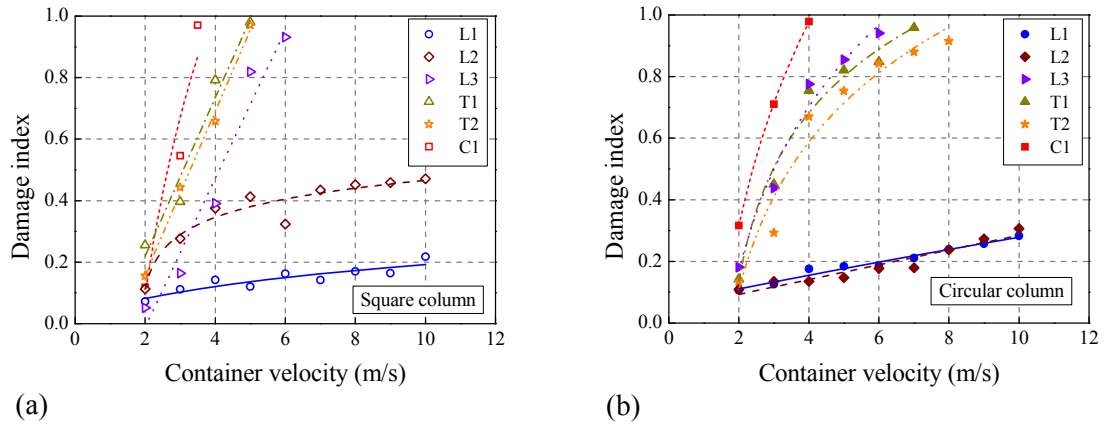


Figure 3.6. Effect of impact configuration on damage behavior of columns impacted by 20' container: (a) square column and (b) circular column.

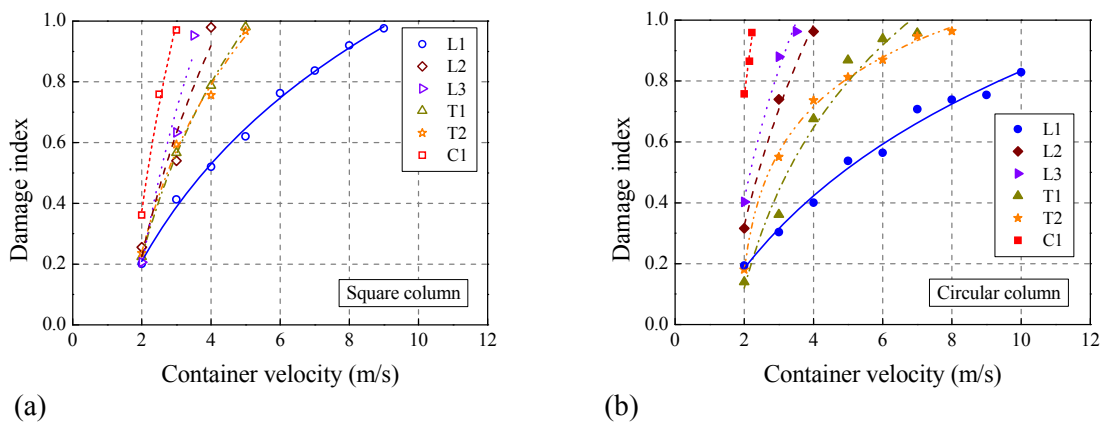


Figure 3.7. Effect of impact configuration on damage behavior of columns impacted by 40' container: (a) square column and (b) circular column.

4. CONCLUSIONS

This paper presents results of an in-depth investigation of RC columns impacted by two types of shipping containers dispersed by a tsunami. It is found that both the impact configuration and shape of the column cross section influence the peak impact force on the column. The square column comes into contact with a wider area of the impacting container, leading to higher impact forces than the circular column. Peak impact force increases with increase of container velocity for both columns. For the 40' container in an impact configuration where stiff members directly resist container deformation, peak impact force is more than three times the corresponding peak impact force for 20' container, although the mass of the 40' container is only 1.7 times larger than the 20' container. This implies that not only mass of the container but also difference in the structural system of the container is significant. For certain impact configurations ASCE 7-10 underestimates the peak impact force for both the columns, particularly, when the stiff members directly resist container deformation. On the other hand, peak impact forces estimated using FEMA P646 are too conservative and differ by an order of magnitude for containers impacting both columns. The impacted column experiences local deformation due to crushing and spalling of concrete at the early stage of contact and the erosion model incorporated in the present analysis can identify these locations. Rapid degradation of axial load carrying capacity is seen in both columns for the impact configurations where stiff members come into contact with the columns. With the increase of container velocity, local deformation is followed by shear deformation of the column with a failure surface across the thickness of the column close to the foundation. Onset of shear failure causes abrupt axial failure of both columns.

ACKNOWLEDGMENT

Financial support from the Center for Urban Earthquake Engineering (CUEE), Tokyo Institute of Technology is gratefully acknowledged.

REFERENCES

- ASCE. (2010). Minimum design loads for buildings and other structures, Standard ASCE/SEI 7-10, American Society of Civil Engineers, Reston, VA.
- ACI. (2008). Building code requirements for structural concrete (ACI 318-08) and commentary, ACI Committee 318, American Concrete Institute, Farmington Hills, MI.
- Belytschko, T., Liu, W. K. and Moran, B. (2000). Nonlinear finite elements for continua and structures, Wiley, New York.
- CEB. (1993). CEB-FIP model code 1990, Comité Euro-International Du Béton, Thomas Telford Services Ltd, Thomas Telford House, London.
- Chock, G., Robertson, I. N., Kriebel, D., Nistor, I., Francis, M., Cox, D. and Yim, S. (2011). The Tohoku, Japan, tsunami of March 11, 2011: effects on structures. EERI special earthquake report, Earthquake Engineering Research Institute, Oakland, CA.
- Containex. (2004). Technical specification. Container-Handelsgesellschaft, <http://www.containex.co.uk/dokumente/567_EN.pdf>.
- Crawford, J. E. and Malvar, L. J. (2006). User's and theoretical manual for K&C concrete model, Report TR-06-19.1, Karagozian & Case, CA.
- FEMA. (2008). Guidelines for design of structures for vertical evacuation from tsunamis. Report FEMA P646, Federal Emergency Management Agency, Washington, DC.
- Jones, N. (1989). Structural impact, Cambridge University Press, Cambridge, UK.
- LS-DYNA. (2007). Keyword user's manual. Livermore Software Technology Corporation, CA.
- Madurapperuma, M. A. K. M. and Wijeyewickrema, A. C. (2012a). Inelastic dynamic analysis of an RC building impacted by a tsunami water-borne shipping container. *Journal of Earthquake and Tsunami*. **6: 1**, 1-17.
- Madurapperuma, M. A. K. M. and Wijeyewickrema, A. C. (2012b). Performance of reinforced concrete columns impacted by water-borne shipping containers. *Advances in Structural Engineering*. (accepted for publication).
- Magellan. (2010). Technical specification for a typical steel dry cargo container. Magellan Maritime Services GmbH, <<http://www.magellan-maritime.de/en/home/technology.html>>.
- Malvar, L. J. (1998). Review of static and dynamic properties of steel reinforcing bars. *ACI Materials Journal*. **95: 5**, 609-616.
- Malvar, L. J., Crawford, J. E., Wesevich, J. W. and Simons, D. (1997). A plasticity concrete material model for DYNA3D. *International Journal of Impact Engineering*. **19: 9-10**, 847-873.
- Malvar, L. J. and Ross, C. A. (1998). Review of strain rate effects for concrete in tension. *ACI Materials Journal*. **95: 6**, 735-739.
- Robertson, I. N., Chock, G. and Morla, J. (2010b). Tsunami effects of the February 27, 2010 Chile earthquake. EERI preliminary reports, Earthquake Engineering Research Institute, Oakland, CA.
- Shi, Y., Li, Z-X. and Hao, H. (2009). Bond slip modelling and its effect on numerical analysis of blast-induced response of RC columns. *Structural Engineering and Mechanics*. **32: 2**, 251-267.
- Tu, Z. and Lu, Y. (2009). Evaluation of typical concrete material models used in hydrocodes for high dynamic response simulations. *International Journal of Impact Engineering*. **36: 1**, 132-146.